

Observations of Tropical Cyclone Structure From WindSat

F. Joseph Turk, *Member, IEEE*, Sabatino DiMichele, and Jeff Hawkins

Abstract—Passive microwave radiometric (PMW) observations of clouds from multichannel imaging sensors onboard low Earth-orbiting environmental satellites are now a vital operational dataset. The first operational passive microwave sensor was the Special Sensor Microwave/Imager onboard the Defense Meteorological Satellite Program satellites, which has been gathering hydrological data records since 1987, and continued with the Tropical Rainfall Measuring Mission (TRMM) and the Advanced Microwave Scanning Radiometer onboard Aqua. These sensors view the underlying scene with an Earth incidence angle near 53° and with a variable azimuthal angle, depending upon the orbit direction and scan position. The WindSat sensor onboard the Coriolis satellite, launched in January 2003, is a five-channel polarimetric PMW radiometer designed to optimize ocean surface wind vector retrievals. While it does not have 85-GHz channels, an added feature is its unique fore-aft viewing capability across a portion of its fore scan swath. This provides a view of the underlying scene from two separate azimuthal directions, which provides added information on the three-dimensional (3-D) structure of clouds and their evolution. In this paper, we compare WindSat and TRMM Precipitation Radar observations of tropical cyclones (TCs) with Monte Carlo radiative transfer simulations performed on idealized 3-D convective cloud structures. The TC 3-D structure and possible tilt in the convective cloud structure are inferred from the difference between the 37-GHz equivalent blackbody brightness temperatures (T_B) from the corresponding fore and aft view observations. The information gained from this analysis is important since asymmetries in the cloud vertical and horizontal structure may be an indication of upper level wind shear, which plays a major role in influencing changes of the TC intensity.

Index Terms—Clouds, cyclone, microwave, radiation, shear, structure, Tropical Rainfall Measuring Mission (TRMM), WindSat.

I. INTRODUCTION

CLOUDS, as well as many terrestrial surface features, appear different to the eye depending upon ones viewing direction. Similarly, passive microwave radiometric (PMW) observations of clouds gathered from moving-platform environmental satellites are different depending upon the sensor

viewing direction in relation to the cloud three-dimensional (3-D) structure at the overpass time. By design, conically scanning passive microwave observations from low Earth-orbiting (LEO) environmental satellites are engineered to provide observations using a nearly constant Earth incidence angle across the scan swath. This greatly simplifies the visual and analytical interpretation of these data over scenes of clouds and radiometrically polarized surface features such as lakes. The first of these operational PMW sensors was the Special Sensor Microwave/Imager (SSM/I) onboard the Defense Meteorological Satellite Program (DMSP) satellites, which have been gathering hydrological data records since 1987, followed by the Tropical Rainfall Measuring Mission (TRMM) Microwave Imager (TMI) and the Advanced Microwave Scanning Radiometer (AMSR-E) onboard the Earth Observing System Aqua satellite in 1997 and 2002, respectively (a similar AMSR on the ADEOS-II satellite gathered data for ten months in 2003).

The 3-D cloud structure affects both the visual interpretation and the quantitative use of PMW data. Since conically scanning PMW radiometers view clouds along a slant path and geolocation coordinates are recorded where the antenna field of view (FOV) intersects the Earth, the imaged cloud location may appear displaced (the displacement largely depends upon the cloud structure and viewing direction). Bauer *et al.* [1] presented a simplified means to correct for the displacement and stretching of equivalent blackbody brightness temperatures (T_B) distributions, noting that the effect is primarily required for higher frequency, higher resolution channels at 37 and 85 GHz. Without accounting for this effect, the underlying rainfall structure or tropical cyclone centering will exhibit a certain degree of positional uncertainty. Plane-parallel radiative transfer models cannot fully describe vertically extended clouds with finite sizes and horizontal inhomogeneities. Haferman *et al.* [2] used a 3-D radiative transfer model to examine the effects of horizontally finite clouds upon precipitation retrieval techniques. Physically, weaker photon interactions (photons escaping) near the cloud edges and downwelling radiation reflected by the surface distort the T_B image from the underlying rainrate distribution. Similar investigations were undertaken by [3]–[5] and more recently by [6]. Since PMW radiometers view clouds from a single direction, there is a certain degree of uncertainty in PMW-based precipitation retrievals owing to the unknown cloud geometry. Turk *et al.* [7] generated simulated TMI satellite images using a mesoscale model simulation of the 1998 Hurricane Bonnie, in order to examine the effect of two satellite viewing directions (180° apart) on a rainfall retrieval algorithm. They noted that the positive differences (overestimates) tended to be spatially adjacent to the negative

Manuscript received February 1, 2005; revised June 8, 2005. This work was supported in part by the Office of Naval Research under Program Element PE-0602435N, in part by the Oceanographer of the Navy through the program office at the PEO C4I&Space/PMW-180 (PE-0603207N), and in part by the National Aeronautics and Space Administration Earth Sciences Division under Grant NNG04HK111.

F. J. Turk and J. Hawkins are with the Marine Meteorology Division, Naval Research Laboratory, Monterey, CA 93943 USA (e-mail: turk@nrlmry.navy.mil).

S. DiMichele is with the European Centre for Medium-Range Weather Forecasts, Reading, RG2 9AX U.K. (e-mail: sabatino.di.michele@ecmwf.int).

Digital Object Identifier 10.1109/TGRS.2006.869926

differences (underestimates), but statistically, the modeled error bounds were consistent with the error bounds from satellite-estimated rainrate data.

By their very nature, moving-platform PMW satellite observations represent snapshots in time and any inferences to dynamical (i.e., time-changing) conditions are indirect. As emphasized in [8], proper interpretation of 85-GHz PMW imagery can reveal information on tropical cyclone (TC) intensity, and with enough PMW overpasses close together in time, an indication of the evolutionary state can often be inferred. If the TC has matured into an eyewall structure, the shape and symmetry of the TC eyewall may be an indication of the surrounding environment, which is known to strongly influence the direction of further TC intensification [9]–[12]. If the synoptic state of the cloud environment (vertical wind shear, inflow, and outflow boundaries, etc.) are strong enough, the combination may produce a preferred direction of the cloud growth, which may be manifested as a tilt or slope in the TC structure. Tilted cloud systems have been investigated in the past. LeMone *et al.* [13] noticed a tilt with height of 20° to 30° from the horizontal in leading edges of convective cloud lines, with steeper tilts amongst individual cloud towers. Hong *et al.* [6] modeled the variability in upwelling T_B due to the presence of tilted convective cloud systems, and using data from the TMI, noticed horizontal displacements between 19- and 85-GHz T_B as large as 100 km. If the underlying scene is a TC with a developed eyewall structure, any satellite-based information that can give an indication of the possible presence of synoptic vertical wind shear conditions is valuable to a TC intensity forecast. In this paper, we extend the studies initiated by Hong *et al.* [6] and Bauer *et al.* [1] to examine whether a PMW radiometer dual-view capability can reveal any added information on tilted cloud structures or other asymmetries, which are not possible from single-view sensors.

In January 2003, the launch of the Coriolis satellite deployed the WindSat sensor into an 833-km altitude low-Earth orbit. WindSat is a 19-channel conically scanning PMW radiometer designed by the Naval Research Laboratory (NRL) [14]. Coriolis orbits in a sun-synchronous pattern with an approximate 6 p.m. local time of ascending node (LTAN), close to the crossing time of the National Aeronautics and Space Administration (NASA) QuikScat satellite. The sensor has full Stokes vector measurement capabilities at 10.7, 18.7, and 37 GHz via direct measurement of vertical (V), horizontal (H), $\pm 45^\circ$, left hand circular (LHC) and right hand circular (RHC) polarized radiation. The channels at 6.8 and 23.8 GHz have V/H measurement capability only. The specifications of the sensor are listed in Table I. The fully polarized channels were designed for PMW-based retrievals of ocean wind vectors, in support of a similar capability which will be available on the National Polar-orbiting Operational Environmental Satellite System (NPOESS) Conical Microwave Imager and Sounder (CMIS) sensor. The wind vector retrievals perform best under cloud-free conditions, and a rain estimation algorithm flags rainy pixels with a quality flag. Unlike other PMW sensors, WindSat records data on both the forward (fore) and back (aft) side of each spin of the conically scanning feedhorn structure. Fig. 1 depicts the conical scanning mode of WindSat. The narrower aft scan data covers a 350-km wide swath, so across a limited region of the fore scan the sensor gathers dual views of

TABLE I
WINDSAT SPECIFICATIONS. EIA = EFFECTIVE INCIDENCE ANGLE,
LHC = LEFT-HAND CIRCULAR, RHC = RIGHT-HAND CIRCULAR,
IFOV = INSTANTANEOUS FIELD OF VIEW

Frequency (GHz)	Channels	EIA (deg)	IFOV (km)
6.8	V, H	53.5	40 x 60
10.7	V, H, $\pm 45^\circ$, LHC, RHC	49.9	25 x 38
18.7	V, H, $\pm 45^\circ$, LHC, RHC	55.3	16 x 27
23.8	V, H	53.0	12 x 20
37.0	V, H, $\pm 45^\circ$, LHC, RHC	53.0	8 x 13

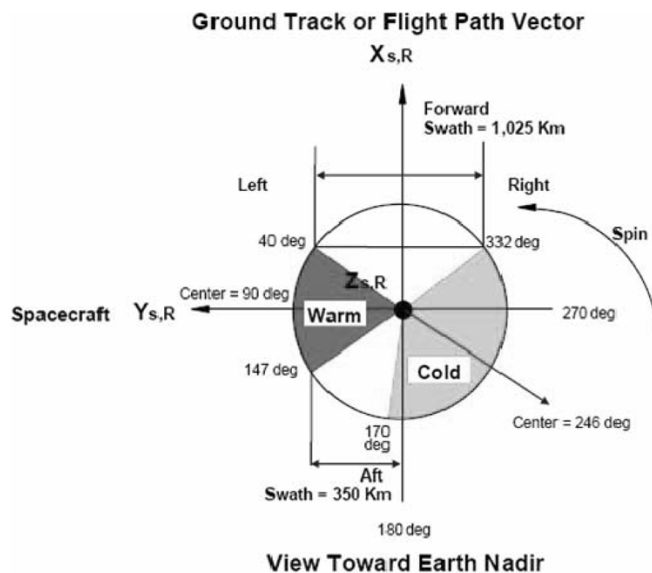


Fig. 1. WindSat scanning geometry. The on-Earth fore- and aft-viewing swath width encompasses 1025 and 350 km, respectively, as the sensor conical scan spins counterclockwise. A dual-view of the same pixel area is possible across the left side of the fore swath with a time offset of approximately 4–5 min, depending upon the across-track beam position (largest time offsets and relative azimuth angles closer to subtrack). Figure adapted from Gaiser *et al.* [14].

the image scene separated in time by 4–5 min, depending upon scan position (smaller time offset near scan edge). Away from subtrack, the relative azimuth between the fore and aft FOVs decreases from near 180° to a minimum of 110° at scan edge.

In this paper, we will examine WindSat overpasses of tropical cyclones to determine the efficacy of its dual-viewing capability to reveal added information on the eyewall structure, shape, and evolution, in lieu of an 85-GHz capability. Independent data from the TRMM Precipitation Radar (PR) and geostationary satellite-estimated vertical wind shear estimates are used to illustrate situations where known shear conditions exist in mature tropical cyclones. Using 3-D Monte Carlo passive microwave radiative transfer simulations of idealized cylindrically shaped tropical cyclone cloud structures, we simulate how the resultant upwelling 37-GHz T_B would appear in both the fore and aft scan directions when a tilt is manifested in the TC eyewall cloud structure. Comparisons of the simulations are made with fore and aft WindSat and TRMM PR observations of tropical cyclones in the Western Pacific Ocean from late 2004. Actual PMW sensor observations provide a coarser scale depiction of the underlying fine-scale cloud variability, and actual

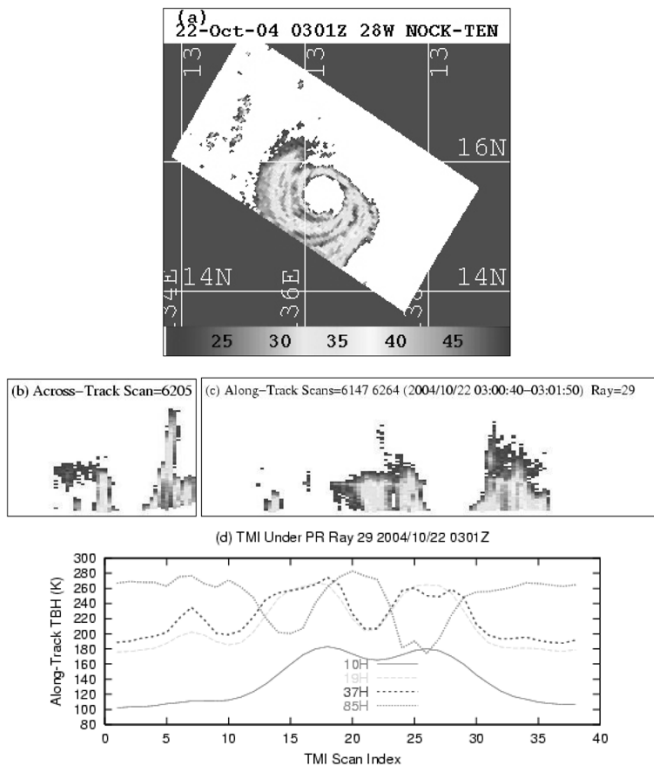


Fig. 2. TRMM descending overpass over tropical cyclone Nock-Ten on October 22, 2004 near 0301 UTC. (a) Map-projected PR attenuation-corrected reflectivity at range gate 70 (near 1-km above surface) in dBZ. Grid lines are spaced every 2° in latitude and longitude. (b) Across-track PR reflectivity profile at scan 6205 (satellite direction is into the paper). Approximate dimensions are 220 km across-track by 20 km height. (c) Along-track PR reflectivity profile between 030040–030150 UTC (satellite direction is left to right). Approximate dimensions are 470 km along-track by 20 km height. (d) Coincident trace of the horizontally polarized T_B at 10, 19, 37, and 85 GHz from the TMI corresponding to the along-track reflectivity profile segment in (c).

TC cloud structures are highly inhomogeneous compared to simplified modeled structures. Nonetheless, taken together the fore-aft (fore minus aft) WindSat and PR observations reveal the spatial features that were shown with the 37-GHz T_B image simulations.

II. EVIDENCE OF TILT IN TROPICAL CYCLONES

One major factor influencing the evolution of tropical cyclones is the state of the local environment, including variables such as the three-dimensional distribution of the wind speed and direction, moisture, sea surface temperature, etc. If a tropical cyclone has already formed, large values of vertical wind shear can weaken or destroy the tropical cyclone by interfering with the internal dynamics and organization of convection [9]. Vertical shear acts to tilt the circulation of the storm, modifying the air-flow throughout. The launch of several key Earth environmental remote sensing satellites in the past decade has greatly improved our capability to monitor the lifecycle of tropical cyclones (TC) [8]. The Precipitation Radar onboard the Tropical Rainfall Measuring Mission (TRMM) satellite was the first spaceborne radar with sufficient sensitivity and vertical and horizontal resolution (250 m and 4 km, respectively) to enable depiction of the 3-D structure of precipitating clouds [15]. While the PR has a small swath and provides a limited number of tropical cyclone eye

TABLE II
ESTIMATED SHEAR MAGNITUDE AND DIRECTION FOR FOUR TROPICAL CYCLONES NEAREST TO THE WINDSAT OVERPASSES DEPICTED IN FIGS. 8, 9, 11, AND 13, RESPECTIVELY. MSLP = MEAN SEA LEVEL PRESSURE. SHEAR DIRECTION IS DEFINED AS DEGREES CLOCKWISE FROM NORTH (E.G., 0 = SHEAR IS DIRECTED FROM NORTH TO SOUTH)

TC Name (Basin)	Date Time	Shear Magnitude (m/s)	Shear Direction (deg)	MSLP (hPa)	Max Winds (knots)	Direction Speed (knots)	Direction Bearing (deg)
Nock-Ten (WPAC)	2004/10/22 06 UTC	6.0	29	949	110	15	290
Meari (WPAC)	2004/09/28 06 UTC	13.8	240	967	75	13	45
Tokage (WPAC)	2004/10/19 18 UTC	16.1	226	976	65	28	30
Nanmadol (WPAC)	2004/12/02 18 UTC	7.8	179	933	110	10	315

overpasses, analysis of long-term data can reveal quantitative information statistically relating cloud properties to tropical cyclone intensity. In a recent study using seven years of PR data, Kelley *et al.* [16] showed that when an eyewall tower is found to exceed a height of 14.5 km, then there was a 71% likelihood of further intensification, but if the maximum height is 10–14.5 km, there was a 46% chance.

Fig. 2 depicts a TRMM descending overpass over typhoon Nock-Ten in the western Pacific Ocean on October 22, 2004 near 0301 UTC. At this time, the typhoon exhibited maximum sustained winds of 100 knots and was moving along a 305° bearing at 11 knots. The top figure depicts a plan view of the PR map-projected attenuation-corrected reflectivity [logarithmic power (dBZ)] at range gate 70 (near 1-km height). The eyewall is nonsymmetric with maximum reflectivities on the left side of the storm (relative to satellite motion), indicative of possible upper level shear. Further motivation for this reasoning is gained by analyzing both the across-track and along-track vertical reflectivity profiles in panels 2 and 3, respectively. The across-track profile shows a tilt toward the south (left side of the storm), indicative of upper level winds blowing from north to south. The along-track profile shows a sloped inner eyewall structure, with a more defined bright band in the east side of the eyewall, indicative of stratiform rain conditions and weaker vertical velocities. Further evidence of the upper level shear is gained from analysis of the University of Wisconsin vertical shear trend analysis [17] tabulated in Table II. These analyses depict vertical wind shear as calculated by subtracting the low-level layer-averaged flow (925–700 hPa) from the upper level layer-averaged flow (300–150 hPa). The magnitude of the vertical shear was estimated to be moderate (6 m/s) along a 29° bearing (from the north), which is in agreement with the suggested direction of eyewall tilt.

The trace of the horizontally polarized T_B from the 10-, 19-, 37-, and 85-GHz channels of the TRMM Microwave Imager (TMI) corresponding to the along-track reflectivity profile are plotted in panel 4. Note that the maximum 10-GHz T_B is offset by about three scans (approximately 45-km) ahead of the 85-GHz minimum near scan 15, but nearly aligned in the more stratiform precipitation band near scan 27. Despite differences in channel resolution, this example shows how differently conically scanning PMW radiometers respond to the presence of tall convective cloud structures at different frequencies, introducing a certain amount of uncertainty in the geolocation of the eyewall position [6].

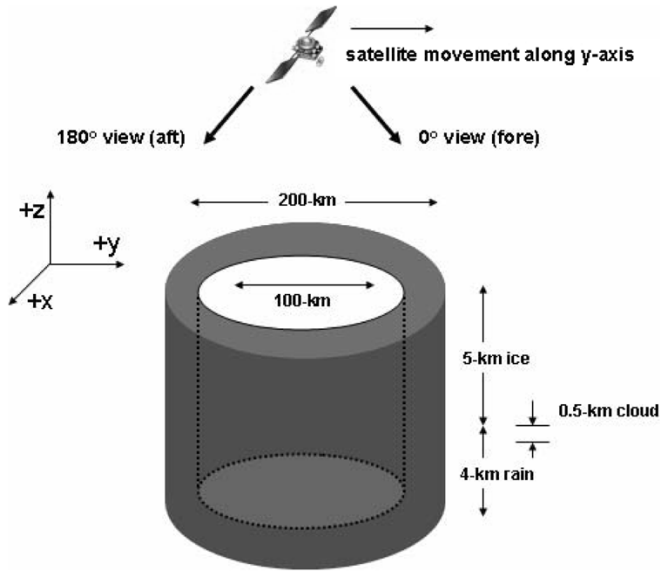


Fig. 3. Three-dimensional perspective view of the structure of the idealized cylindrical tropical cyclone. The simulated satellite moves along the $+y$ axis and views the structure along the fore (0° azimuth) and aft (180° azimuth) directions, with a 53° satellite zenith angle. The inner and outer diameters are 100 and 200 km, respectively. A 5-km ice layer is atop a 4-km rain layer, with a 0.5-km layer of nonprecipitating cloud liquid water coexisting at the top of the rain layer. A tropical water vapor profile is superimposed extending from the surface up to 20 km in approximately 1-km layers.

As depicted in Fig. 1, if the storm lies on the left side of the WindSat swath (relative to satellite motion), then the WindSat sensor will be able to provide multiple views of the storm from its fore and aft scans. In particular, there may be discernable differences between the fore and aft views within the finest resolution 37-GHz Image Data Record (IDR) data (see Table I) related to cyclone structure. In the next section, we use Monte Carlo simulations to determine if information in the fore-aft differences can be related to cyclone eyewall tilt, and hence indicate a change in the cyclone intensity due to the presence of vertical shear conditions.

III. DUAL-VIEW SIMULATIONS

In order to simulate the 37-GHz fore-aft viewing observations available from WindSat, 3-D radiative transfer computations were performed using the backward Monte Carlo simulator originally developed in [3] and later used in [6] and [18]. This method follows received photons backward through the medium in a probabilistic manner, whereby photons are either scattered or absorbed at each interaction. A simplified Henyey–Greenstein phase function is used to determine the direction of travel after each scattering event. The radiative properties of all hydrometeors are computed using Mie theory and exponential drop size distributions, and a tropical radiosonde profile gathered during the 1993 TOGA–COARE experiment is superimposed [19]. The ocean surface emissivity is assumed to be Fresnel (smooth water surface) with a surface temperature of 300 K. The horizontal grid dimensions are 80×80 with a 5-km grid spacing, and 20 1-km layers in the vertical. Only horizontally polarized modeling was done, both for brevity and the lower ocean surface emissivity provides a wider T_B dynamic range for cloud scenes.

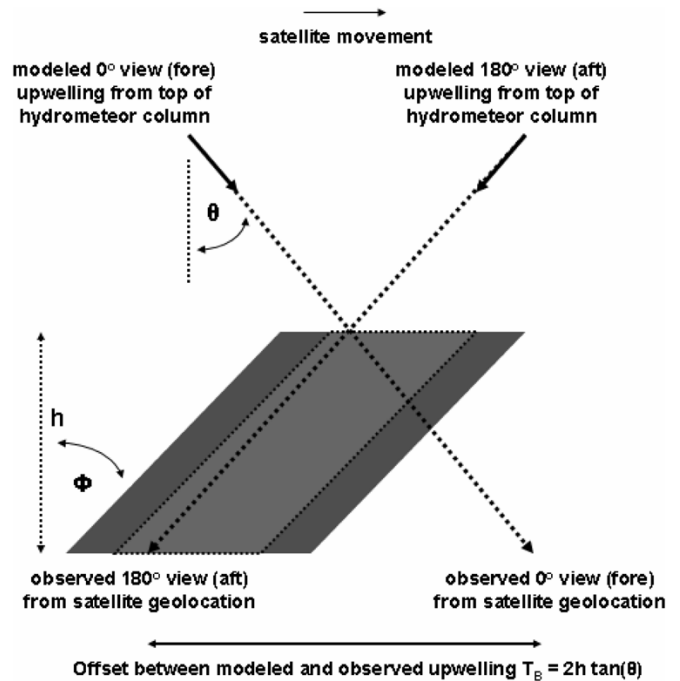


Fig. 4. Side-view (along-track) depiction of the structure of the simulated tilted cyclone, using a $\Phi = 45^\circ$ tilt along the y axis. While radiative transfer simulations report the upwelling 0° and 180° azimuth radiances from the same position on TOA, a conically scanning satellite sensor observation viewing the same TOA point (zenith angle denoted by θ) is positioned further ahead along the sensor view direction. The atmosphere height where the majority of the radiometric signal response originates is denoted by h .

Fig. 3 depicts the simplified cylindrical cloud structure used to model a tropical cyclone. The 45° tilted cloud model structure described in [6] is used. The inner and outer diameters are 100 and 200 km, respectively. A 5-km ice layer (density $= 0.9 \text{ g} \cdot \text{cm}^{-3}$) is placed atop a 4-km rain layer (rain liquid water content $= 3 \text{ g} \cdot \text{m}^{-3}$), where a 0.5-km layer of cloud liquid water (cloud liquid water content $= 0.5 \text{ g} \cdot \text{m}^{-3}$) is superimposed from 3.5 to 4 km height. The simulated satellite along-track direction is from left to right in this figure (x axis is across-track and the y axis is along-track). In Fig. 4, an along-track side-view depiction of the tilted structure is shown, where a $+45^\circ$ tilt has been applied along the y axis. The radiative transfer simulations were first performed at 85 GHz for the nontilted and tilted structures, in order to test and replicate the previously published results of [6].

Fig. 4 also points out differences between model simulations and actual satellite observations that must be taken into account if these two datasets are to be properly compared. Radiative transfer simulations are usually coded to report the upwelling radiances from the top of the atmosphere (TOA), but satellite sensor observations are geolocated at the coordinates where the center of the (IFOV) intersects the Earth. For conically scanning instruments, this introduces an geolocation offset as shown in Fig. 4. In these cases, the radiative transfer simulations report the upwelling 0° and 180° azimuth radiances from the same position on TOA, but a satellite sensor observation viewing along the same azimuthal directions would have its radiances reported as the on-Earth intersection point of the IFOV beam. This offset will be taken into account when comparing fore-aft (fore minus aft) modeled differences, so that the simulated two-dimensional

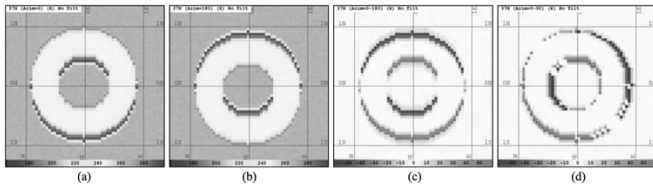


Fig. 5. Simulated upwelling T_B from the nontilted cyclone structure in Fig. 3. In all figures, azimuthal = 0° is defined as viewing from the bottom toward the top, and azimuth = 90° is viewing from left to right. In all panels, the latitude and longitude grid lines are spaced 1° apart. From left to right: (a) upwelling 37-GHz horizontally polarized T_B for a satellite zenith angle of 53° and azimuth viewing angles of 0° , (b) azimuthal viewing angle of 180° , (c) 0° to 180° T_B difference, and (d) 0° to 90° T_B difference.

T_B images can be properly compared to WindSat images. For the 5-km horizontal grid, a satellite zenith angle of 53° and a 9-km cloud top, this works out to an approximate four-pixel offset between fore and aft, applied along the viewing direction.

In Fig. 5, the simulated upwelling 37-GHz T_B from the nontilted cyclone structure is depicted for a satellite zenith angle of 53° and azimuthal viewing angles of 0° [Fig. 5(a), left panel] and 180° [Fig. 5(b), middle panel], and the 0° to 180° T_B difference [Fig. 5(c), right panel]. As you look at these figures, azimuth = 0° is defined as viewing from the bottom toward the top, and azimuth = 90° is viewing from left to right. In other words, the simulated satellite is moving from top to bottom. The background upwelling T_B is near 200 K owing to emission from water vapor and cloud liquid water alone. For reference, the eye is positioned at a location of (0°N , 0°E), and grid lines are spaced every 1° in latitude and longitude.

For the 0° case of Fig. 5(a), the viewing direction first intersects the rain layer leading to a rapid T_B warming near 290 K against the radiometrically cool ocean background. As the view intersects, the ice layer and radiation from the rain and cloud layers are scattered away from the viewing direction, the upwelling T_B cools to a minimum of near 240 K. Near the upper edge of the eyewall, the T_B cools to near 190 K over a small region (10 K cooler than the background, since the beam is intersecting only the ice layer, and the 200-K background radiation is slightly reduced by scattering within the ice) before settling to the 200-K background value. A similar process occurs on the other side of the cyclone eyewall. Since the structure is radially symmetric, the 0° and 180° T_B images are mirror images of each other, and the 0° to 180° T_B difference (fore-aft) image in panel 3 shows thin alternating positive and negative bands near both the upper and bottom edges of the cyclone eyewall, with differences near ± 40 K.

In Fig. 6, the cyclone is tilted by 45° along the direction of the negative y axis (i.e., slanted toward the bottom in these figures). The panels are otherwise identical with Fig. 5. With this configuration, the tilted eyewall is nearly aligned along the 0° azimuthal view. Therefore, the 0° azimuthal view [Fig. 6(a), left panel] intersects the ice layer first, and very quickly the T_B rises to the same 240-K maximum as in Fig. 5(a). A separate thin band of $T_B \approx 230$ K is evident below 1° S, which is caused by the warm emission from the rain layer reflecting off of the ocean surface and into the view direction. The band of radiometrically warm $T_B \approx 290$ K appears near the lower edge of eyewall center (near 0.4° S latitude). Even though the view is transversing a path through the high-albedo ice layer, the closer

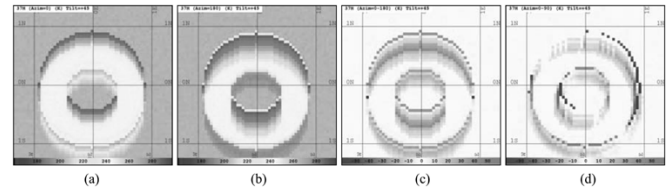


Fig. 6. Same as Fig. 5, but the cyclone is tilted by 45° along the direction of the negative y axis (i.e., slanted toward the bottom in these panels).

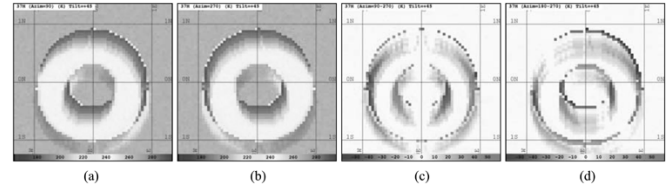


Fig. 7. Same tilted structure as Fig. 6, but for (a) azimuth viewing angle of 90° , (b) azimuthal viewing angle of 270° , (c) the 90° to 270° T_B difference, and (d) the 180° to 270° T_B difference.

the view is to the eyewall edge, there is a greater probability for the photons to escape into the surrounding atmosphere, which reduces the overall probability of scattering back along the simulated FOV. Along the top (north side) of the eyewall, the effect is similar—warming due to reflection of rain emission, scattering of the rain layer by the ice layer, then a weakening of the scattering effect near the upper cloud edge allowing more of the warm rain emission to pass through.

In Fig. 6(b), the 180° azimuthal view, similar types of explanations hold, but the view now first intersects the radiometrically warm rain layer for a longer distance, leading to a gradual T_B warming to ≈ 290 K, then a cooling to 240 K. The band of 190 K is also evident (10 K cooler than the background) as noted in Fig. 5(b), but a wider band here owing to the tilt. On the bottom (south side), the effect is similar—the region of ≈ 290 K is smaller since it is resulting from emission inside rather than outside of the eyewall, but the band of 190 K (below 1° S) is wider since it is resulting from weak ice scattering along the outer eyewall perimeter. The net result is that the 0° to 180° T_B difference image [Fig. 6(c)] shows a more widespread, weaker intensity (differences of only ± 20 K) pattern of alternating positive and negative bands near both the upper and bottom edges of the cyclone eyewall (the “ribbon” around the inner and outer perimeters is an artifact, owing to the fact that the offset used to on-Earth align the 0° and 180° azimuthal view images is limited by the horizontal grid spacing of 5 km).

In Fig. 7, we illustrate the situation of azimuth viewing angles of 90° [Fig. 7(a), left panel] and 270° [Fig. 7(b), middle panel], and the 90° to 270° T_B difference [Fig. 7(c), right panel]. In other words, the satellite is moving from left-to-right. This simulates the situation where the eyewall is tilted to the right of the forward viewing direction. The net result in the 90° to 270° T_B difference image [Fig. 7(c)] appears to be a similar widespread pattern of alternating positive and negative bands, symmetric (in absolute value) about the y axis, with differences near ± 40 K. However, the features are not symmetric about the x axis and the T_B differences are larger on the side of the tilt (south side).

We also have analyzed the behavior of the 0° to 90° and 180° to 270° T_B differences (90° relative azimuth), which is closer to the actual WindSat fore-aft azimuth difference at swath

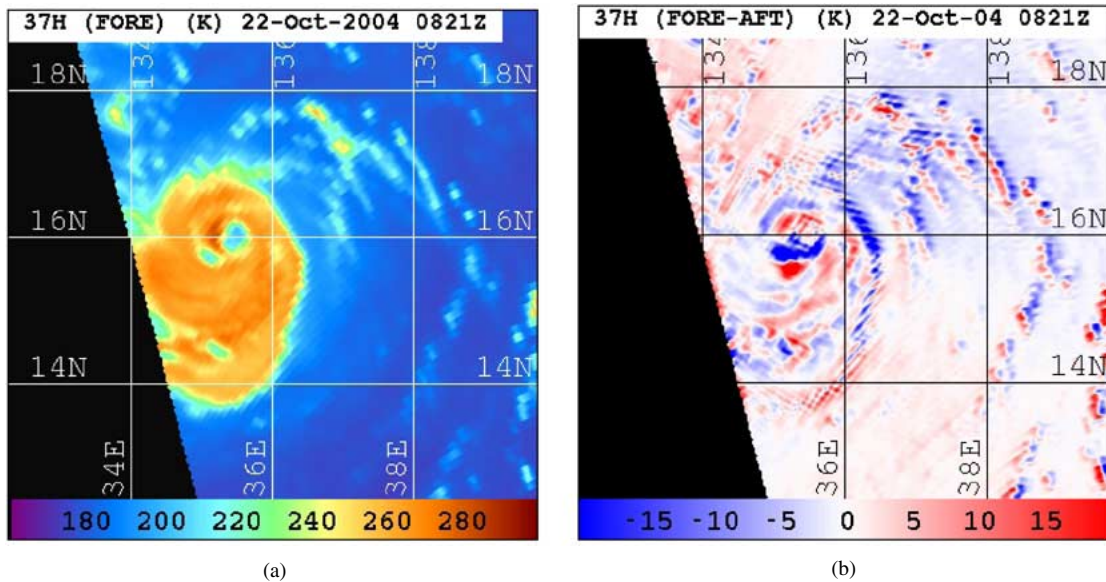


Fig. 8. (a) 37H channel from the WindSat ascending overpass over typhoon Nock-Ten centered at 0821 UTC on October 22, 2004. Color scale is in Kelvin. (b) Associated 37H-GHz T_B difference between the fore- and aft-viewing scans. The scale extends from ± 20 K in an anomaly scale where red and blue intensities indicate positive and negative, respectively. In all panels, the latitude and longitude grid lines are spaced 2° apart.

edge (near 110° when the scene is near the left edge of the swath). Figs. 5(d), 6(d), and 7(d) depict these corresponding cases, with and without tilt. The net effect is to render the T_B differences less symmetric about either the 0° or 180° direction. In Fig. 5(d), the maximum inner eyewall negative and positive differences appear to the left of subtrack and along subtrack, respectively. The combination of a 90° azimuthal offset and a $+45^\circ$ tilt [Figs. 6(d) and 7(d)] is to spread out or “blur” the T_B structure from that of the nontilted structure.

The idealized cylindrical cloud structures used here are necessary simplifications of the more complex, time-evolving 3-D shapes of tropical cyclones [20]. The magnitudes of the T_B depicted in these simulations are a function of the TC microphysical vertical structure. While fore-aft differences appear whenever a cloud edge is detected, the overall pattern of the fore-aft difference is dependent upon the direction of tilt relative to the satellite motion. In reality, corresponding WindSat fore and aft views maintain a near-constant zenith angle but are viewed from a different azimuth across-track; only the pixels near subtrack possess relative azimuth differences near 180° . Nonetheless, the simulations show that the WindSat fore-aft data may provide some added evidence regarding the presence, strength and direction of eyewall tilt (either across-track or along-track of the satellite motion). In the next section, we analyze WindSat overpasses of several tropical cyclones to observe how their fore-aft differences compare with the theoretical calculations of this section.

IV. COMPARISONS WITH WINDSAT OBSERVATIONS

As shown in Fig. 1, the fore-aft capability of WindSat extends over a portion of the left side of the forward scan. Scenes near subtrack have time offsets near 5 min, and scenes captured near swath edges have smaller relative azimuth angles (near 110° at swath edge) and time offsets, whereas the model simulations assume a 180° azimuthal viewing difference and no storm evolution. Therefore, when the fore and aft images

are differenced there is a slight horizontal displacement that occurs due to natural storm advection throughout the time interval between fore and aft views. In the dynamic TC environment, the displacement distance is on the order of one 37-GHz pixel (10 km). We assume that the resulting radiometric difference is much less than that owing to the radiometric difference due to the different viewing paths. It is important to keep in mind that unlike 85-GHz observations, 37-GHz over-ocean T_B are dual-valued (i.e., similar T_B can result from emission warming or scattering-induced T_B depressions), which can appear to distort the shape of the eyewall structure unless taken into account. Also, if a predominant ocean surface wind direction is present, a certain amount of fore-aft difference over less optically thick clouds will be evident. However, this signal is only several Kelvin compared to the > 10 K fore-aft signal owing to clouds.

In Fig. 8(a), the 37H (horizontal polarization) channel image from the 0821 UTC WindSat ascending overpass over typhoon Nock-Ten on October 22, 2004 is shown. These data are mapped onto a 2-km per-pixel rectangular map projection to smooth the image representation. At this stage in its evolution Nock-Ten was estimated to have maximum winds of 110 knots, moving along a 290° bearing at about 15 knots. From Table II, the magnitude of the vertical shear was estimated to be 6 m/s along a 29° bearing (from the north). While the corresponding TRMM image of Fig. 2 was captured nearly 5 h earlier, a similar organization of the asymmetric eyewall structure is evident, with the majority of the typhoon development to the south. The associated 37H-GHz T_B difference between the fore- and aft-viewing scans is shown in Fig. 8(b) (anomaly scale extends between ± 20 K, where red and blue indicate positive and negative differences, respectively). The main eyewall shows magnitudes of positive and negative differences exceeding ± 20 K on the southern side, with weaker magnitudes of near ± 10 K on the north side. The comparison with Figs. 5(c) and 6(c) suggests that the eye may be tilted toward the south (as suggested by the TRMM PR profiles of Fig. 2, with deeper, more convective

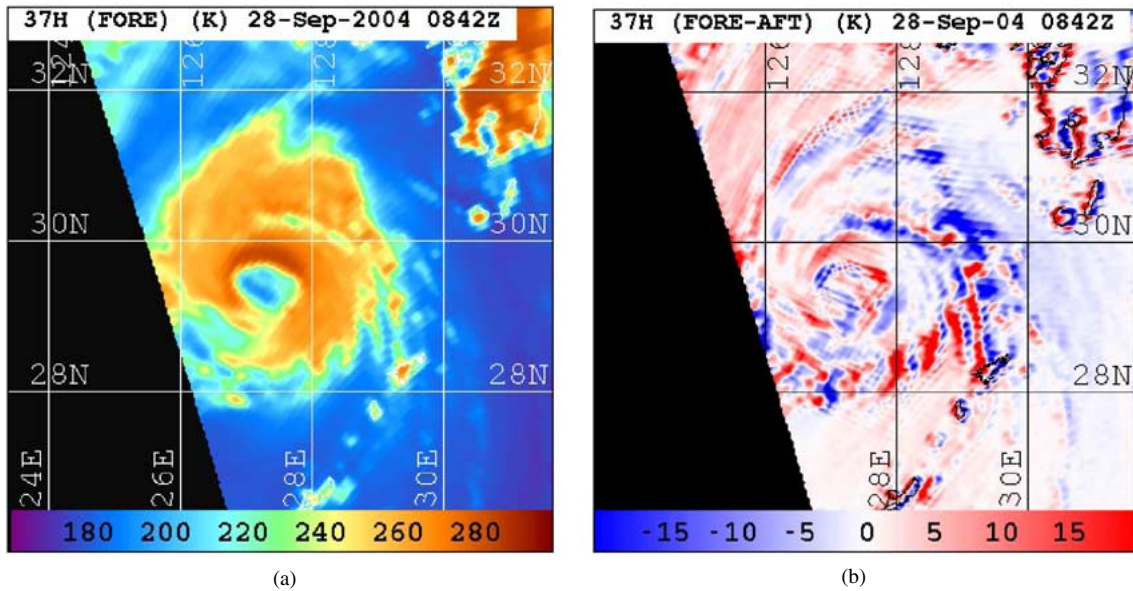


Fig. 9. Same as Fig. 8, but for the WindSat ascending overpass over typhoon Meari centered at 0841 UTC on September 28, 2004.

clouds to the south), as well as the wind shear direction estimate provided in Table II (moderate shear from the north). However, given inherent scale differences between model simulations and satellite observations, and the vertical extent of the clouds, it is difficult to conclude anything definite on the magnitude of the tilt. The tilt appears quite small in this storm, which is at an intense phase (110 knot winds) such that the shear would have to be much stronger in order to impart any deintensification. Additionally, the storm is close to the left edge of the swath as the satellite ascends, so the relative azimuth between the fore and aft scans is closer to 130°.

Fig. 9 shows another example, the WindSat ascending overpass over typhoon Meari centered at 0841 UTC on September 28, 2004. At this stage in its evolution, Meari had estimated maximum winds of 75 knots, moving toward the northeast at about 13-knots toward the southern Japanese islands. From Table II, the magnitude of the vertical shear was estimated to be 13.8 m/s along a 240° bearing (from the southwest toward the northeast). The eyewall structure is asymmetric, wider in diameter with main development on the north side, which is in accord with these strong vertical shear estimates, indicative of a storm being weakened by shear. The preferred cloud direction is evident in the TRMM overpass at 0852 UTC (11 min after the WindSat overpass) in Fig. 10. The PR vertical radar reflectivity profiles show a vertical structure oriented to the left (relative to satellite motion) in the across-track profile and to the right (in the direction of motion) in the along-track profile, indicative of the northeasterly directed shear. The 85-GHz T_B minimum is only near 220 K and occurs near TMI scan 33, after the 10-GHz T_B has reached its maximum near TMI scan 28 (bottom panel of Fig. 10). The Windsat fore-scan views the front edge (emission from rain layer in the tilted cloud and lack of significant ice) first, providing positive fore-aft differences [Fig. 9(b)] over the north side of the eyewall near 30N latitude. The north side of the eyewall exhibits mainly widespread positive differences, smaller in magnitude than the example in Fig. 8(b). From Fig. 6(a) and (b), the effect of the tilt is to spread out the area of positive-negative difference and

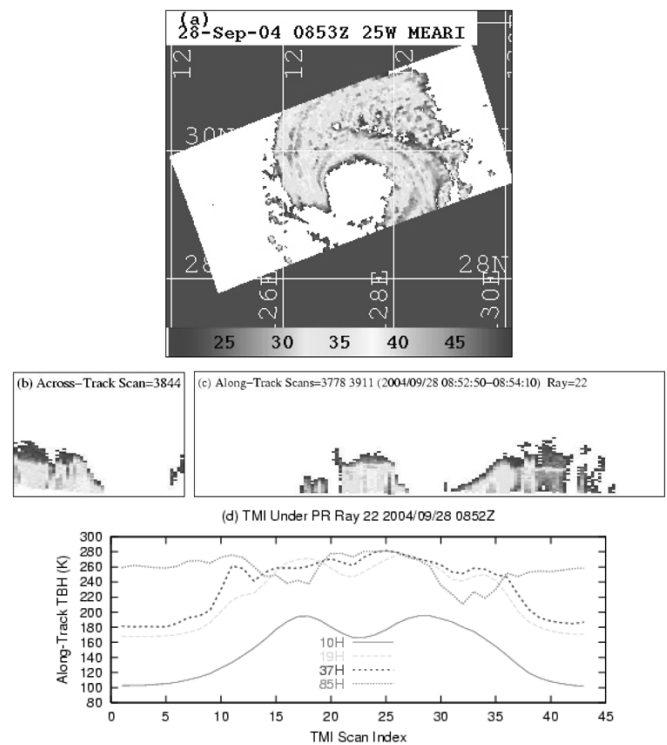


Fig. 10. Same as Fig. 2, but for the TRMM ascending overpass over typhoon Meari centered at 0852 UTC on September 28, 2004 (11 min after the WindSat overpass shown in Fig. 9).

reduce the absolute magnitude. The weaker intensity compared to typhoon Nock-Ten (75 versus 110 knots) and the PR profiles of Figs. 2 and 10 suggests that shear effects are stronger in this example. We note how Fig. 9(b) contrasts with Fig. 8(b), which was from a more intense typhoon with nearly circularly shaped red/blue (positive and negative) areas and which, theoretically, would indicate much less tilt. Note that the blue-red ribboning effect at coastlines is a manifestation of the fact that the fore and aft pixels are never exactly viewing the same scene. The orientation of the fore and aft pixel is different, such that they

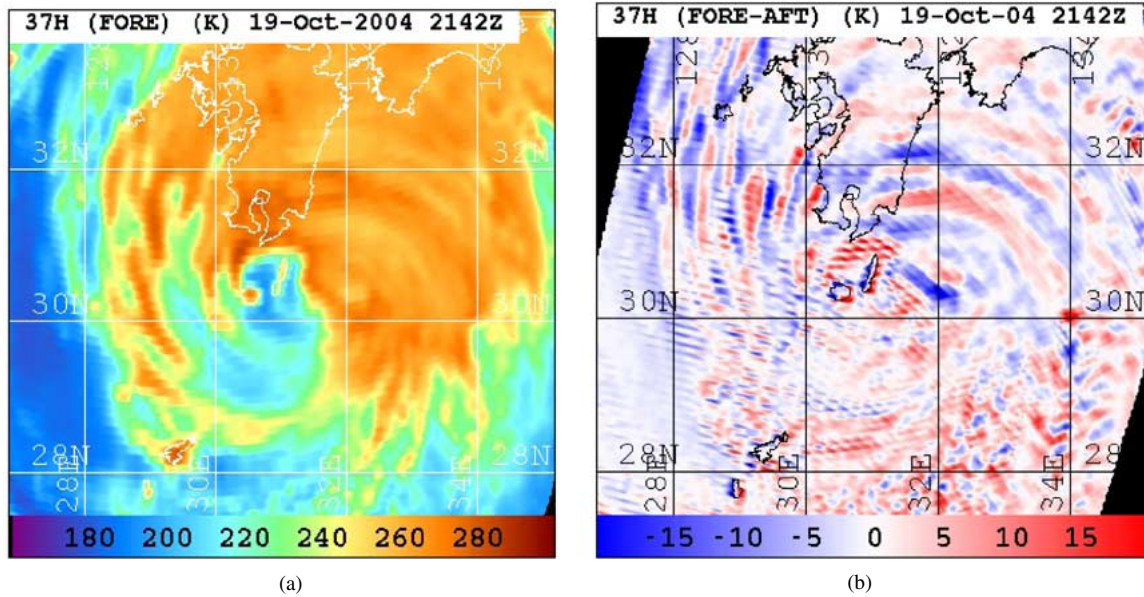


Fig. 11. Same as Fig. 8, but for the WindSat descending overpass over typhoon Tokage centered at 2142 UTC on October 19, 2004.

each intersect a different amount of radiometrically cold ocean and radiometrically warm land, leading to a positive fore-aft difference at some pixel locations, others negative.

The final two examples are shown in Figs. 11–14, which depict two descending WindSat overpasses and their corresponding nearest time TRMM overpasses. Fig. 11 shows the 2142 UTC WindSat descending overpass over typhoon Tokage on October 19, 2004, moving along a 30° bearing toward Japan. The TRMM ascending overpass in Fig. 12 occurred near 2219 UTC, 37 min after this WindSat overpass. Fig. 13 is the 2222 UTC WindSat descending overpass over typhoon Nanmadol on December 2, 2004, moving along a 315° bearing after crossing the Philippine Islands (it would soon curve to the northeast and move over Taiwan). The TRMM ascending overpass in Fig. 14 occurred near 2229 UTC, 7 min after this WindSat overpass.

In both of these cases, the majority of the cloud development is on the north side of the eyewall structure. From Table II, the shear is directed toward the northeast (Tokage) and north (Nanmadol), which is in accord with these observations. Tokage had the strongest vertical shear (estimated at near 16 m/s) and weaker intensity of the two. In both Figs. 11(b) and 13(b), near the eye the fore-aft differences are not as well defined and rather weak. The 85-GHz AMSR-E imagery from the 1732 UTC (4 h earlier, not shown) Aqua overpass over Tokage also show the eyewall being sheared apart. If tilt is toward the north as these data suggest, near the inner eyewall edge the fore-aft differences would first be negative [inner blue area in Fig. 6(c)], since the aft scan would be peering into the side of the tilted cloud (radiometrically warm emission, since the majority of the ice top has been sheared away). The negative values are noticeable in the north side of the eyewall in Fig. 11(b) (just touching the southernmost tip of the Japanese island of Kyushu). The along-track PR profile of Tokage in Fig. 12 shows the shear as a general slope in the cloud structure, and the strongest 85-GHz ice scattering signatures of $T_B < 200$ K further away from the eye.

For typhoon Nanmadol (Figs. 13 and 14), the storm is at a stronger intensity (110 knots), and shear is moderate at 7.8 m/s, directed from south to north (Table II), in accord with the struc-

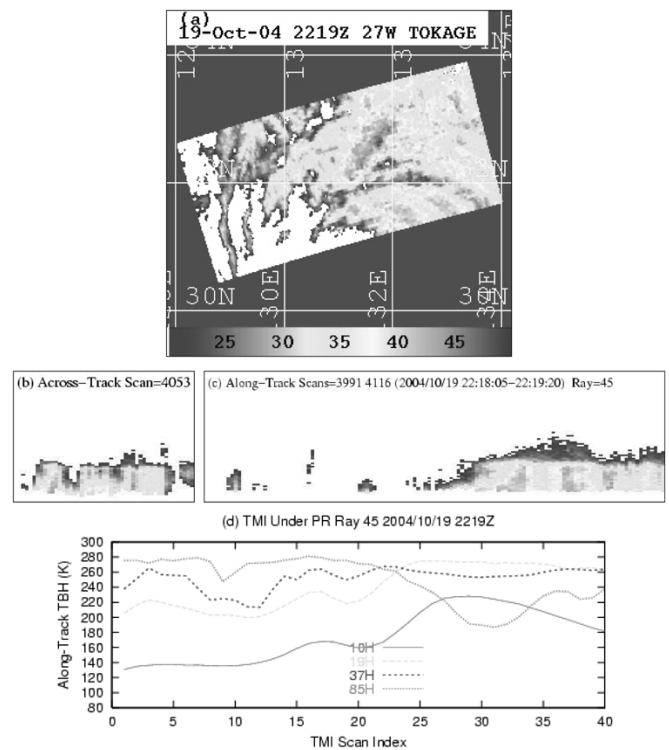


Fig. 12. Same as Fig. 2, but for the TRMM ascending overpass over typhoon Tokage centered at 2219 UTC on October 19, 2004 (37 min after the WindSat overpass shown in Fig. 11).

ture depicted in Fig. 13. This would lead one to expect mainly negative fore-aft differences on the north side of the eyewall with a descending WindSat overpass. For the descending pass shown in Fig. 13(b), the negative fore-aft differences in the inner eye are indeed noticed just above 18° latitude. The along-track PR profile shown in Fig. 14 also shows the slanted inner eyewall structure, which is not as dramatic as that noted from typhoon Tokage, but expected with the smaller estimated vertical shear of typhoon Nanmadol.

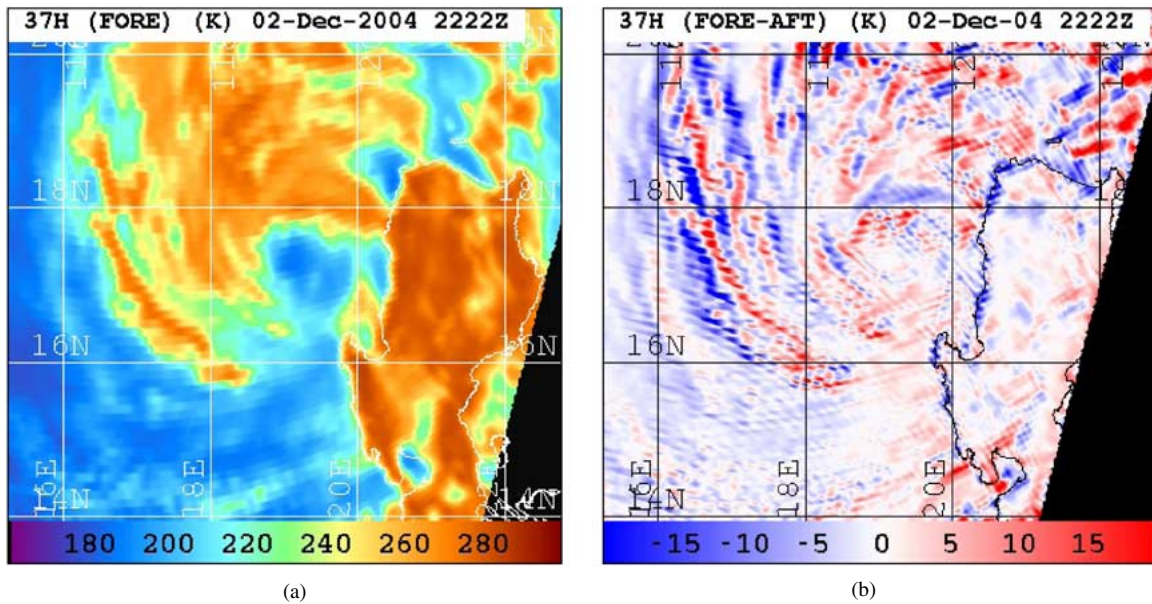


Fig. 13. Same as Fig. 8, but for the WindSat descending overpass over typhoon Nanmadol centered at 2222 UTC on December 2, 2004.

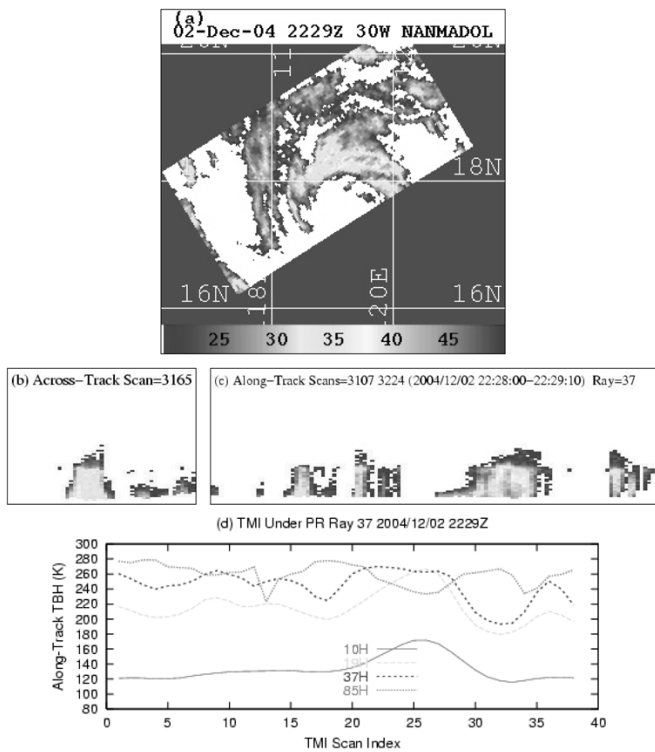


Fig. 14. Same as Fig. 2, but for the TRMM ascending overpass over typhoon Nanmadol centered at 2229 UTC on December 2, 2004 (7 min after the WindSat overpass shown in Fig. 13).

V. CONCLUSION

In this paper, we used a combination of 3-D microwave radiative transfer simulations and WindSat and TRMM observations of tropical cyclones in an attempt to determine if the unique fore and aft viewing capabilities of the WindSat

passive microwave radiometer could be used to characterize TC structure, asymmetry, and tilt in eyewall structures. WindSat lacks 85-GHz capabilities previously shown to be instrumental for TC intensity inferences. However, it has 37-GHz capability, and its fore and aft scans view along different directions. Previous studies have suggested that the presence of a tilt owing to upper level shear in the surrounding environment may be indicative of an ongoing change in the tropical cyclone intensity. Using nearest time overpass data from the Precipitation Radar onboard TRMM, we examined typhoons in the western Pacific Ocean from late 2004 that depicted sheared eyewall structures and compared them to independently produced vertical shear analyses from geostationary cloud and water vapor-tracked winds. Three-dimensional microwave radiative transfer simulations were performed at 37 GHz using simplified vertical and tilted cylindrically shaped TC structures to simulate fore and aft sensor viewing. While the modeling is an oversimplification of the complex cloud geometries and microphysical richness found in various stages of TC evolution, it did reveal unique radiometric features that differed depending upon the presence and direction of a preferred tilt in the cloud structure.

Observations from four different typhoons of varying state (intensity and maximum winds) were analyzed, and the WindSat fore-aft differences were compared to the vertical shear estimates, TRMM-PR observations, and with the 3-D Monte Carlo radiative transfer simulations. In all cases, the radar vertical reflectivity profiles from the PR were in agreement with the direction of the (independently estimated) vertical shear estimates. The complex microphysical structure of a TC in relation to the fixed height, ideally shaped clouds used in Section III makes quantitative model-satellite T_B intercomparison difficult. In all scenes, WindSat 37-GHz fore-aft T_B differences appear most predominantly near sharp cloud gradients and cloud edges. Near the eyewall edges, the position and sign (positive or negative, depending upon

the direction of tilt relative to the satellite direction) of the 37-GHz WindSat fore-minus-aft T_B difference demonstrated reasonable agreement with the values that would be associated with the direction of tilt suggested from vertical shear estimates and nearby TRMM overpasses. While this investigation has been of a limited nature (four examples), it does suggest that there is potential to utilize WindSat 37-GHz fore-aft data for analysis of cloudy scenes. In particular, the fore-aft data shows potential to identify (at a minimum) which quadrant has the preferred direction of tilt or shear in a tropical storm, which could be augmented with (other) nearby-time 85-GHz data from other satellites (TMI, AMSR-E, SSM/I) to better define storm intensification (or deintensification) trends.

The dual-viewing capability of WindSat was originally devised to improve passive radiometric ocean surface wind vector estimates, where the presence of clouds is an obstruction to the quality of wind vector retrievals. In this work we have showed that the dual-viewing may be potentially useful for characterization of the structure of convective clouds within and surrounding tropical storms. In addition to the more qualitative aspects studied here, the dual-view capability may also assist in establishing improved error characterization in PMW-based precipitation retrieval algorithms owing to unknown cloud geometry variations, especially for 85-GHz observations [7], [21]. This latter work may have implications and relevance to algorithm design and implementation in the future NASA Global Precipitation Measurement mission.

ACKNOWLEDGMENT

The first author would like to thank G. Poe (Naval Research Laboratory) for his many informative suggestions regarding the interpretation of WindSat data, and to C. Velden (University of Wisconsin) for his assistance with vertical wind shear data and interpretation. The authors thank J. Tesmer (Navy Fleet Numerical Meteorological and Oceanographic Center) for the WindSat data and the NASA TRMM Science Data and Information Service for the TRMM data.

REFERENCES

- [1] P. Bauer, L. Schanz, and L. Roberti, "Correction of three-dimensional effects for passive microwave remote sensing of convective clouds," *J. Appl. Meteorol.*, vol. 37, pp. 1619–1632, 1998.
- [2] J. Haferman, E. N. Anagnostou, D. Tsintikidis, W. F. Krajewski, and T. F. Smith, "Physically based satellite retrieval of precipitation using 3-D passive microwave radiative transfer model," *J. Atmos. Ocean. Technol.*, vol. 13, pp. 832–850, 1996.
- [3] L. Roberti, J. Haferman, and C. D. Kummerow, "Microwave radiative transfer through horizontally inhomogeneous precipitating clouds," *J. Geophys. Res.*, vol. 99, pp. 16707–16718, 1994.
- [4] Q. Liu, C. Simmer, and E. Ruprecht, "Three-dimensional radiative transfer effects of clouds in the microwave spectral range," *J. Geophys. Res.*, vol. 101, pp. 4289–4298, 1996.
- [5] G. W. Petty, "Area-average solar radiative transfer in three-dimensionally inhomogeneous clouds: The independently scattering cloudlet model," *J. Atmos. Sci.*, vol. 59, pp. 2910–2929, 2002.
- [6] Y. Hong, J. L. Haferman, W. S. Olson, and C. D. Kummerow, "Microwave brightness temperatures from tilted convective systems," *J. Appl. Meteorol.*, vol. 39, pp. 983–998, 2000.

- [7] F. J. Turk, S. Di Michele, P. Bauer, F. S. Marzano, A. Mugnai, L. Roberti, A. Tassa, and P. Gaiser, "Precipitation retrieval from dual-view spaceborne passive microwave radiometers," presented at the *Int. Radiation Symposium (IRS-2004)*, Busan, Korea, Aug. 23–28, 2004.
- [8] J. D. Hawkins, T. F. Lee, J. Turk, C. Sampson, J. Kent, and K. Richardson, "Realtime internet distribution of satellite products for tropical cyclone reconnaissance," *Bull. Amer. Meteorol. Soc.*, vol. 82, no. 4, pp. 567–578, 2001.
- [9] G. Gallina, "Environmental vertical wind shear and tropical cyclone intensity change utilizing enhanced satellite derived wind information," M.S. thesis, Atmos. and Ocean. Dept., Univ. Wisconsin, Madison, 2002.
- [10] J. A. Knaff, S. A. Seseske, M. DeMaria, and J. L. Demuth, "On the influences of vertical wind shear on symmetric tropical cyclone structure derived from AMSU," *Mon. Weather Rev.*, vol. 132, pp. 2503–2510, 2004.
- [11] S. C. Jones, "On the ability of dry tropical-cyclone-like vortices to withstand vertical shear," *J. Atmos. Sci.*, vol. 61, pp. 114–119, 2004.
- [12] M. DeMaria, J. A. Knaff, and B. H. Connell, "A tropical cyclone genesis parameter for the tropical Atlantic," *Weather Forecast.*, vol. 16, pp. 219–233, 2001.
- [13] M. A. LeMone, G. M. Barnes, E. J. Szoke, and E. J. Zipser, "The tilt of the leading edge of mesoscale tropical convective lines," *Mon. Weather Rev.*, vol. 112, no. 3, pp. 510–519, 1984.
- [14] P. W. Gaiser, K. M. St. Germain, E. M. Twarog, G. A. Poe, W. Purdy, D. Richardson, W. Grossman, W. L. Jones, D. Spencer, G. Golba, J. Cleveland, L. Choy, R. M. Bevilacqua, and P. S. Chang, "The WindSat spaceborne polarimetric microwave radiometer: Sensor description and early performance," *IEEE Trans. Geosci. Remote Sens.*, vol. 42, no. 11, pp. 2347–2361, Nov. 2004.
- [15] C. D. Kummerow, "The status of the Tropical Rainfall Measuring Mission (TRMM) after two years in orbit," *J. Appl. Meteorol.*, vol. 39, pp. 1965–1982, 2000.
- [16] O. A. Kelley, J. Stout, and J. B. Halverson, "Tall precipitation cells in tropical cyclone eyewalls are associated with tropical cyclone intensification," *Geophys. Res. Lett.*, vol. 31, pp. 25 112–25 115, 2004.
- [17] C. S. Velden, C. M. Hayden, S. Nieman, W. P. Menzel, S. Wanzong, and J. Goerss, "Upper-tropospheric winds derived from geostationary satellite water vapor observations," *Bull. Amer. Meteorol. Soc.*, vol. 78, pp. 173–195, 1997.
- [18] S. Di Michele, A. Tassa, A. Mugnai, F. S. Marzano, P. Bauer, and J. P. V. P. Baptista, "Bayesian algorithm for microwave-based precipitation retrieval: Description and application to TMI measurements over ocean," *IEEE Trans. Geosci. Remote Sens.*, vol. 43, no. 4, pp. 778–791, Apr. 2005.
- [19] E. A. Smith, J. Turk, M. R. Farrar, and X. Xiang, "Estimating 13.8 GHz path integrated attenuation from 10.7 GHz brightness temperatures for the TRMM combined PR-TMI precipitation algorithm," *J. Appl. Meteorol.*, vol. 36, pp. 365–388, 1997.
- [20] G. Panegrossi, S. Dietrich, F. S. Marzano, A. Mugnai, E. A. Smith, X. Xiang, G. J. Tripoli, P. K. Wang, and J. P. V. P. Baptista, "Use of cloud model microphysics for passive microwave-based precipitation retrieval: Significance of consistency between model and measurement manifolds," *J. Atmos. Sci.*, vol. 55, pp. 1644–1673, 1998.
- [21] C. D. Kummerow, Y. Hong, W. S. Olson, S. Yang, R. F. Adler, J. McCollum, R. Ferraro, G. Petty, D. B. Shin, and T. T. Wilheit, "The evolution of the goddard profiling algorithm (GPROF) for rainfall estimation from passive microwave sensors," *J. Appl. Meteorol.*, vol. 40, pp. 1801–1817, 2001.



F. Joseph Turk (M'80) received the B.S. and M.S. degrees in electrical engineering from Michigan Technological University, Houghton, and the Ph.D. degree from Colorado State University, Fort Collins, in 1982, 1984, and 1991, respectively.

From 1984 to 1986, he was with Motorola, Inc., Schaumburg, IL. Since 1995, he has been with the Marine Meteorology Division, Naval Research Laboratory, Monterey, CA. His areas of expertise are in passive and active microwave remote sensing related to clouds and precipitation, multisensor satellite techniques, radiative transfer modeling, satellite data assimilation, and the role of precipitation in climate. He is a member of the NASA Precipitation Missions Science Team.

Sabatino Di Michele received the laurea degree in electronic engineering and the Ph.D. degree in information and electrical engineering from the University of L'Aquila, L'Aquila, Italy, in 1997 and 2004, respectively.

Since the beginning of 1998, he has been collaborating with the Department of Electrical Engineering, University of L'Aquila, working on SSM/I applications and ground-based radiometry. In November 1998, he joined the Institute of Atmospheric Physics, CNR, Rome, Italy, to work on rainfall retrieval techniques for the Tropical Rainfall Measuring Mission (TRMM) microwave instruments. He is currently with the European Centre for Medium-range Weather Forecast (ECMWF), Reading, U.K., working on issues related to rainfall assimilation. He has been participating in various international projects (e.g., EuroTRMM, Eurainsat) concerning precipitation estimation from spaceborne microwave sensors. He is also involved in the research activity of the planned Global Precipitation Measurement Mission. His studies are mainly focused on radiative transfer modeling and on the development of new inversion procedures.

Jeff Hawkins received the B.S. and M.S. degrees in meteorology from the Florida State University, Tallahassee, in 1976 and 1979, respectively, with an emphasis in synoptic meteorology.

In 1979, he began his long-term interest in tropical cyclone (TC) research with what is now the National Oceanic and Atmospheric Administration's Hurricane Research Division, Miami, FL, by participating in the SeaSat scatterometer and SMMR validation onboard P-3 hurricane hunters. He has worked for 25 years at the Naval Research Laboratory, first as a Satellite Oceanographer (Stennis Space Center, MS) and the last 13 years as a Satellite Meteorologist in Monterey, CA, with a heavy emphasis on passive microwave signals from intense TCs. His current research interests include understanding TC structure changes during eyewall replacement cycles and the creation of novel satellite products to assist Navy real-time nowcasting/forecasting applications.

Mr. Hawkins is a Fellow and recipient of a Special Award from the American Meteorological Society, recipient of the Navy's Meritorious Civilian Service Award, and member of two National Academy of Science panels.